RESEARCH ARTICLE

NANO · MICRO small
www.small-journal.com

Bioinspired Omnidirectional Interface Engineered Flexible Island for Highly Stretchable Electronics

Osman Gul, Myoung Song, Chang-Yeon Gu, Jihyeon Ahn, Kichul Lee, Taek-Soo Kim, Junseong Ahn, Hye Jin Kim,* and Inkyu Park**

With the advancement of electronics, there is a growing need to effectively combine rigid, flexible, and stretchable materials to build hybrid electronics. However, the interfacial transition between rigid/flexible and stretchable substrates presents considerable challenges, mainly due to differences in elastic moduli, complicating their integration for practical usage. Here, bioinspired omnidirectional interfacial-engineered flexible islands (BOIEFI) are introduced for a robust transition from flexible to stretchable substrates. These BOIEFIs enable the creation of highly stretchable and durable hybrid substrates capable of withstanding diverse physical deformations such as stretching, twisting, and even poking. Inspired by plant roots, BOIEFIs are designed with primary and secondary root structures that provide flexible mechanical interlocking between substrates with different elastic moduli. Through experimental and computational methods, optimized BOIEFIs exhibit significantly enhanced stretchability and improved fatigue life. To demonstrate the broad applicability, light-emitting diodes (LEDs) are integrated into BOIEFIs to establish a stretchable display. In addition, a human-machine interface device with soft pressure sensors and an LED array is fabricated for the implementation of hybrid electronics. This approach facilitates the harmonious integration of rigid, flexible, and stretchable substrates, leading to the creation of soft, highly stretchable, and durable hybrid electronics.

1. Introduction

Stretchable electronics have received significant attention owing to potential widespread applications in electronic skins, displays, and haptic devices.[1–7] These electronics, also known as hybrid electronics, typically consist of rigid/flexible parts that integrate conventional electronic components and protect them from mechanical stimuli, as well as stretchable parts that accommodate mechanical deformation.[8,9] Therefore, to realize reliable stretchable electronics, it is essential to consider not only the individual rigid or stretchable substrates but also their interfacial regions because differences in elastic moduli between parts can lead to delamination issues.

Several structural and material-based approaches have been established to address these interfacial modulus mismatch problems.[10–15] Techniques such as serpentine and kirigami designs utilize flexible substrates like polyimide (PI) or polyethylene terephthalate (PET), patterning them to be stretchable through structural modifications.[16–23] However, these structure-based approaches exhibit low stretchability (≈50%) and demonstrate irreversible behavior under excessive stretching. Another widely used approach is the material gradient method,[24–29] which creates a smooth modulus gradient from the rigid part to the stretchable part using various materials or composites. Despite its popularity, this integration still faces interfacial failure and delamination problems under stretching because fabricating a perfectly smooth modulus gradient with different materials is highly challenging. A more recent approach,[30] the interfacial engineering method, creates stretchable electronics by combining stretchable and rigid substrates with a mechanical interlocking effect (Table S1, Supporting Information). Although this strategy shows great potential because it can reliably connect rigid/flexible and stretchable parts, accommodating strains of up to several hundred percent, it still faces challenges such as a lack of mechanism analysis, nonuniform stress transitions, and limited electrically available areas. Therefore, it is crucial to understand the mechanisms at the interface and optimize the interfacial regions to enable practical applications of hybrid electronics that integrate rigid, flexible, and stretchable substrates. This

O. Gul, M. Song, C.-Y. Gu, J. Ahn, K. Lee, T.-S. Kim, I. Park
Department of Mechanical Engineering
Korea Advanced Institute of Science and Technology (KAIST)
291 Daehak-ro, Daejeon, Yuseong-gu 34141, Republic of Korea
E-mail: inkyu@kaist.ac.kr

O. Gul, H. J. Kim
Intelligent Components and Sensors Research Section
Electronics and Telecommunication Research Institute (ETRI)
218 Gajeong-ro, Daejeon, Yuseong-gu 34129, Republic of Korea
E-mail: nolawara@etri.re.kr

J. Ahn
Department of Control and Instrumentation Engineering
Korea University
Sejong 30019, Republic of Korea
E-mail: junseong@korea.ac.kr

H. J. Kim
Department of Advanced Device Technology
University of Science and Technology
Daejeon 34113, Republic of Korea

The ORCID identification number(s) for the author(s) of this article can be found under https://doi.org/10.1002/smll.202410247

DOI: 10.1002/smll.202410247

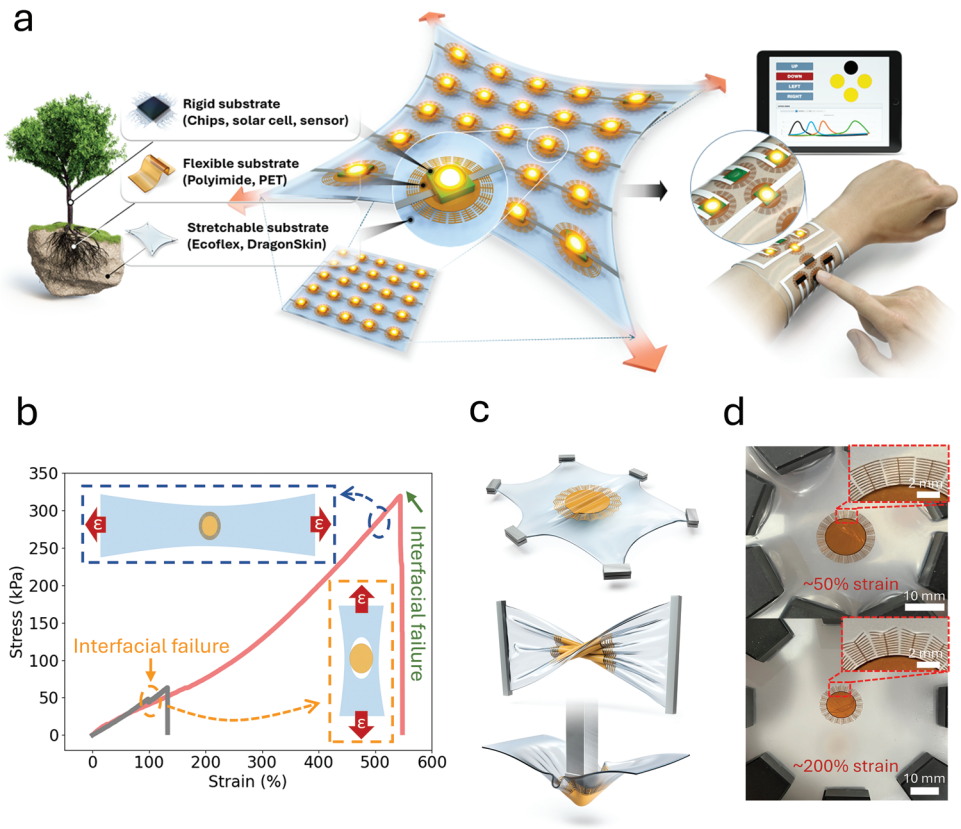

Figure 1. Bioinspired omnidirectional interface-engineered flexible islands (BOIEFI) within stretchable substrate for hybrid electronics. a) Schematic illustration of stretchable hybrid electronics with BOIEFI. b) Stress versus strain comparison for the rootless circle island (RCI) (gray curve) and BOIEFI (red curve) embedded in Ecoflex under stretching. c) Schematic illustration of BOIEFI within stretchable substrate under physical deformation modes such as strain, twisting, and poking d) Up: photographs of BOIEFI within stretchable substrate under omnidirectional 50% strain; Down: photographs of BOIEFI within stretchable substrate under omnidirectional 200% strain.

understanding is key to advancing the fields of electronic skin, displays, and haptic devices by integrating rigid and stretchable sensors.[31–34]

Here, we propose bioinspired omnidirectional interface-engineered flexible islands (BOIEFI) for integrating rigid, flexible, and stretchable substrates, achieving high stretchability and demonstrating outstanding performances under physical deformations for hybrid electronics. Plants anchor themselves firmly by gripping the soil with their roots. The roots spread widely and deeply, providing support and stability to the plants. In addition, the root structure also protects the rigid plant body from external forces such as wind and erosion. Inspired by this structure and its functions, we developed an interfacial engineering approach for rigid/flexible-to-stretchable substrates by mimicking the primary and secondary root structures of plants (**Figure 1a**). A comprehensive parametric analysis was performed on primary and secondary roots to analyze and optimize the BOIEFI design. The optimized BOIEFI exhibited a significant improvement in stretchability, achieving up to 540% elongation under uniaxial tensile testing, facilitated by its flexible mechanical locking mechanism. This result highlights the system's ability to accommodate high strains along a single axis without failure. (Figure 1b; Figures S1 and S2, Supporting Information). Moreover, this mechanism extends the lifespan of the developed hybrid electronics platform under various physical deformations, including strain, poking, and twisting (Figure 1c,d). The developed hybrid electronics platform effectively integrates rigid, flexible, and stretchable substrates. The successful integration of diverse substrates using BOIEFI interfaces is demonstrated through a stretchable light-emitting diodes (LEDs) array and a stretchable human-machine interface device (s-HMI Device) with soft pressure sensors and rigid LEDs. The s-HMI device provides remote control and visual directional information, functioning similarly to keyboard directional inputs.

2. Results and Discussion

2.1. Design and Fabrication of the BOIEFI

Polyimide (PI) (Young's modulus: 3.2 GPa),[22] which is widely used as a material for flexible electronics, and Ecoflex (Young's modulus: 50 kPa),[35] which is known for its highly stretchable properties, are used to create the flexible-to-stretchable interface for BOIEFI. The design of the BOIEFI is inspired by the way plants anchor themselves into the soil with their roots. Specifically, the primary and secondary roots of the plant anchoring system are meticulously mimicked and integrated into the design to create BOIEFI (**Figure 2a**). First, primary roots are positioned

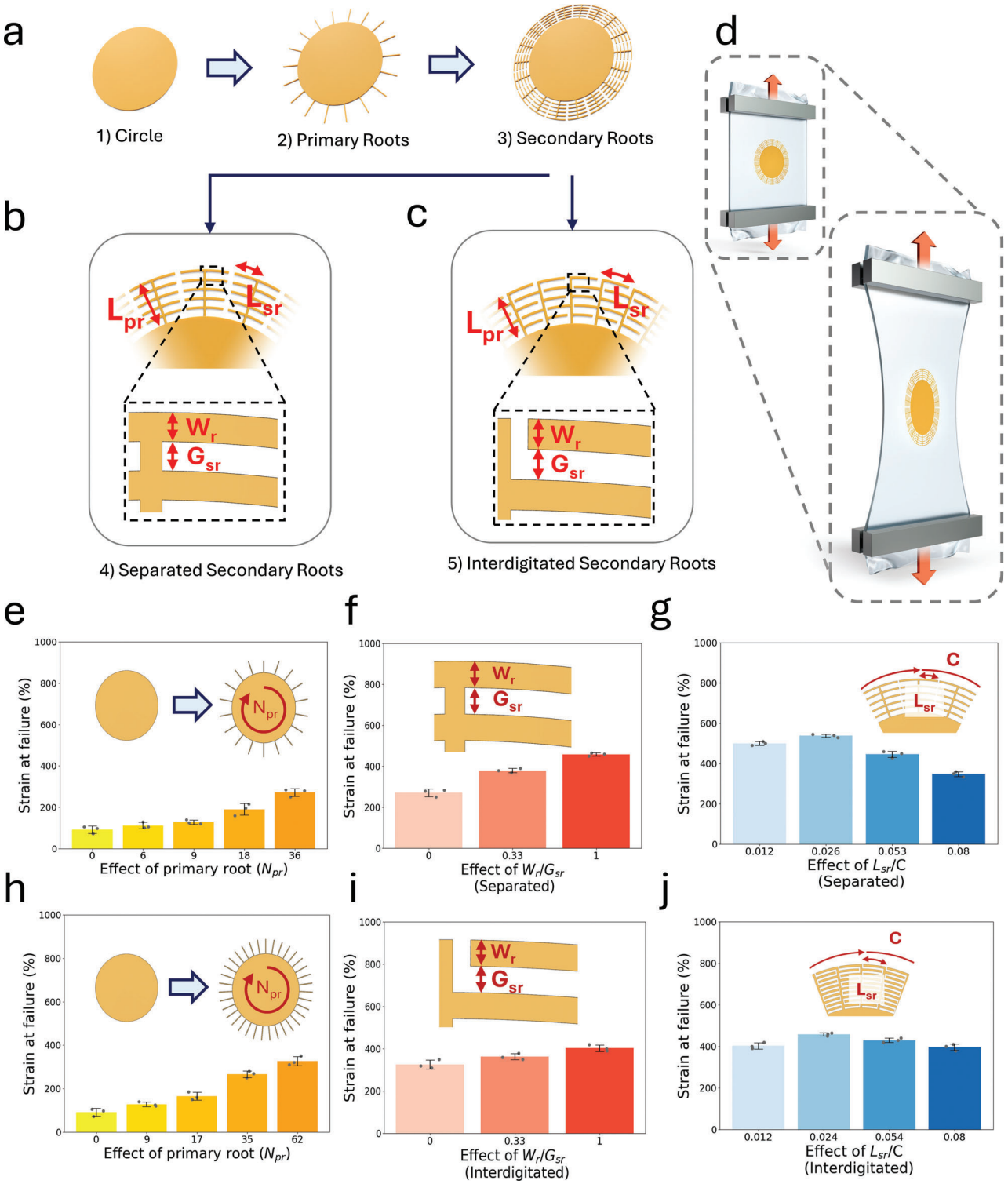

Figure 2. BOIEFI designs, parameter study, and results. a) Schematic illustration of the procedure for creating BOIEFI. b) Parameters of BOIEFI of separated root design c) Parameters of BOIEFI of interdigitated root design: primary root length: L_{pr}, secondary root length: L_{sr}, gap between secondary roots: G_{sr}, root width: W_r. d) Schematic illustration of strain experiment test set-up for BOIEFI. e) Experimental results of the effect of primary roots in the strain at failure for separated root design. f) Experimental results of the effect of the ratio of root width and spacing between roots (W_r/G_{sr}) for separated root design. g) Experimental results of the effect of the ratio of secondary root length to circumference (L_{sr}/C) for separated root design. h) Experimental results of the effect of primary roots in the strain at failure for interdigitated root design. i) Experimental results of the effect of the ratio of root width and spacing between roots (W_r/G_{sr}) for interdigitated root design. j) Experimental results of the effect of the ratio of secondary root length to circumference (L_{sr}/C) for interdigitated root design. Error bars indicate standard deviations (sample number = 3).

in a circular 360° configuration of a circle to enhance the omnidirectional stress distribution effect. Second, secondary roots are arranged perpendicular to the primary roots. The secondary root system functions as a flexible mechanical interlocking mechanism, preventing crack propagation by anchoring effectively into the stretchable material. Two distinct root designs are proposed to investigate their effects: a separated root design and an interdigitated root design. The separated root design has a single primary root with secondary roots branching out symmetrically on both sides (Figure 2b). Conversely, in the interdigitated root design, the secondary roots are arranged to interlock with each other in an interdigitated design (Figure 2c).

The BOIEFI design incorporates both constant and variable parameters to explore the effects of design parameters. The radius of the rootless circle island (R_{rci}) and the length of the primary root (L_{pr}) are fixed at 5 and 2 mm, respectively, as constant parameters. The secondary root length (L_{sr}), root width (W_r), gap between the secondary roots (G_{sr}), number of primary roots (N_{pr}), and number of secondary roots (N_{sr}) are strategically chosen as variable parameters to optimize the BOIEFI design. Additionally, the circumference of the BOIEFI design is denoted as the C value. To achieve equal spacing and a balanced design for the parameter study, Equations (1–5) can be formulated.

$$C = 2 \times \pi \times R_{rci} \tag{1}$$

$$L_{sr,\ separated} \approx \frac{C - 2 \times N_{pr} \times W_r}{2 \times N_{pr}} \tag{2}$$

$$L_{sr,\ interdigitated} \approx \frac{C - 2 \times N_{pr} \times W_r}{N_{pr}} \tag{3}$$

$$L_{pr,\ separated} = (W_r + G_{sr}) \times N_{sr} \tag{4}$$

$$L_{pr,\ interdigitated} = (W_r + G_{sr}) \times 2 \times N_{sr} \tag{5}$$

The circumference can be calculated using Equation (1). The length of separated secondary roots ($L_{sr,\ separated}$) can be determined by Equation (2), while the length of interdigitated secondary roots ($L_{sr,\ interdigitated}$) can be calculated using Equation (3). Equations (4) and (5) define the formulation for the root width, the gap between secondary roots, and the number of secondary roots in the cases of separated and interdigitated secondary root designs, respectively.

The BOIEFI specimens are fabricated using a UV laser-cutting machine to precisely cut PI material. The detailed fabrication procedure is illustrated in Figure S3 (Supporting Information) and elucidated in the Experimental Section. To define the interfacial failure quantitatively, strain at failure is measured depending on the root design (Figure 2d). The detailed test method is described in the Experimental Section.

2.2. Parameter Study and Optimization of the BOIEFI

To investigate the separated and interdigitated root design cases under similar parametric values and their effect on the strain at failure value, the design parameters [N_{pr}, L_{sr}/C, and W_r/G_{sr}] were established. The relation between the length of the secondary root and the island's circumference ratio was established as the ratio of L_{sr}/C to investigate its effect on strain at failure. Also, the relation between the secondary root width and spacing between roots was established as the ratio W_r/G_{sr} to investigate the optimal ratio for strain at failure value. The design code follows the format of (parameter abbreviation)(value). For example, N_{pr}36 denotes that the primary root number is 36.

Prior to conducting the experiments, several initial assumptions were made to ensure a fair and efficient parameter study. The L_{sr}/C and W_r values for both separated and interdigitated root designs were initially set to be equal to examine the impact of secondary root design on strain at failure. By specifically establishing the L_{sr}/C ratio and W_r, the number of primary roots (N_{pr}) is determined by the given Equations (2–5), allowing for the investigation of the effect of the primary root number for both separated and interdigitated root designs. Initially, the root width was set to 100 µm to establish the design parameters. Considering the radius of the circle, and the consistent L_{sr}/C ratio for both the separated and interdigitated root designs, the maximum values for N_{pr} were selected as 36 for the separated root design and 62 for the interdigitated root design, respectively (Equations 2 and 3). Then, experiments for N_{pr} were conducted to investigate the strain at failure for primary roots (Figure 2e–h).

First, the separate root design was systematically investigated to evaluate its mechanical behavior and effect on stretchability. With N_{pr} set to a maximum of 36, the strain at failure value was investigated from N_{pr}0 to N_{pr}36. While the RCI showed a strain at a failure value of 90%, N_{pr}36 exhibited a strain at a failure value of ≈260% (Figure 2e). Here, an increase in the number of primary roots also increased the strain at failure values, indicating that primary roots help to distribute stress in the flexible-to-stretchable interface. Then, to investigate the effect of the width of the secondary root on the strain at failure value, the widths of the roots chosen for investigation were 70, 100, and 200 µm while the number of secondary roots (N_{sr}) was set to 5. Notably, 70 µm represents the minimum achievable width in the fabrication process. The G_{sr} value for each width is calculated using Equation (4). While a root width of 100 µm showed the maximum strain at a failure value of 440%, a root width of 70 µm exhibited the lowest strain at a failure value of 265% (Figure S4, Supporting Information). Here, note that the width of the roots affects the failure mode of the flexible-to-stretchable interface. Up to 100 µm, the secondary roots exhibited a flexible mechanical interlocking effect. Beyond 100 µm, however, the secondary roots lost their flexibility and demonstrated a rigid mechanical interlocking effect. This change in failure mode was observed through experiments, as depicted in Figure S5 (Supporting Information). Specifically, widths up to 100 µm resulted in a peeling failure mode for the flexible-to-stretchable interface. In contrast, widths of 200 µm, characterized by rigid mechanical interlocking, led to fracture failure. Therefore, for further experiments, the width of the secondary root was fixed at 100 µm. When the ratio of W_r/G_{sr} was equal to 1, it showed the maximum strain at a failure value of 465%, which was chosen as the constant value for the further parameter experiments (Figure 2f). To optimize the design parameters for BOIEFI, the secondary root length has

shown significant importance as demonstrated by experiments (Figure 2g). The previously established secondary root length, calculated using Equation (2), was utilized for further investigations. A longer secondary root length tended to decrease the strain at failure value. Conversely, if the secondary root length was smaller than a certain value ($L_{sr}/C = 0.026$), it also led to a decrease in the strain at failure value. This suggests that there is an optimal value ($L_{sr}/C = 0.026$) that enhances the gripping effect of BOIEFI. In summary, to optimize the separated root design, we conducted an extensive parameter study on N_{pr}, W_r, W_r/G_{sr}, and L_{sr}/C.

Second, to compare both separated and interdigitated root designs, the same optimization process used for the separated root design was conducted for the interdigitated root design (Table S2 and Figure S3, Supporting Information). To maintain similar design parameter values as the separated root design, the primary root number for the interdigitated root design was set to $N_{pr}9$, $N_{pr}17$, $N_{pr}35$, and $N_{pr}62$ which were calculated using Equation (3). For these N_{pr} values, the corresponding L_{sr}/C ratios were selected to match the values used in the separated root design, ensuring that the comparison between the two designs was based on similar geometric conditions. This allows for a more direct evaluation of how the interdigitated root design affects strain at failure while keeping the L_{sr}/C ratio consistent with the separated design. As confirmed before, as the number of primary roots in the design increases, the strain at failure value also increases. The $N_{pr}62$ design demonstrated the highest strain at a failure of 320% (Figure 2h). The $N_{pr}62$ design was then chosen to conduct W_r/G_{sr} parameter experiments. The G_{sr} value for each width is calculated using Equation (5) for interdigitated root design. When the W_r/G_{sr} ratio reached 1, it showed the highest strain at a failure value of ≈400% (Figure 2i). With W_r/G_{sr} equal to 1, this value was set as constant for the L_{sr}/C experiment. As a result, the strain at failure values for L_{sr}/C values of 0.012, 0.024, 0.054, and 0.08 were 403%, 456%, 430%, and 396%, respectively (Figure 2j). We observed that, in the case of the interdigitated root design, the strain at failure value increased up to 460% when the L_{sr}/C value reached 0.024. However, beyond this point, the strain at failure value decreased. This indicates that an L_{sr}/C value of ≈0.024 achieved the optimized result for stretchability in the interdigitated root design case.

The same optimization process for separated and interdigitated root designs was conducted to identify the optimized BOIEFI configuration. By systematically adjusting and comparing key parameters, such as N_{pr}, L_{sr}/C, and W_r/G_{sr} for both designs, the goal was to determine the most effective configuration for maximizing strain at failure. A correlation study was conducted since the W_r/G_{sr} and L_{sr}/C values were similar in both design cases. When the W_r/G_{sr} value reached 1, the separated root design exhibited higher strain at the failure value (Figure S6, Supporting Information). Conversely, when the L_{sr}/C ratio was 0.08, the interdigitated design showed higher strain at the failure value. However, when the ratio reached 0.026, the separated root design showed the highest strain at failure value. Beyond the values of 0.024 and 0.026, both designs exhibited a decrease in strain at failure value (Figure S7, Supporting Information). With the parameter and correlation studies, we can conclude that the separated root design demonstrates extraordinary stretchability with its optimized structure ($N_{pr} = 18$, $W_r/G_{sr} = 1$, $L_{sr}/C = 0.026$). This comparison allowed for a direct evaluation of how these geometric parameters influence the strain at failure in the separated and interdigitated root designs. By maintaining consistent ratios between these critical parameters, the study provided insights into how each design performs under similar conditions, enabling a more accurate determination of the optimal structure for stretchability. Additionally, the effect of varying modulus on strain at failure was analyzed. Dragon Skin 10 demonstrated nearly twice the stiffness of Ecoflex 0030. While the RCI structure exhibited a strain at a failure of 46%, the BOIEFI structure achieved a significantly higher strain at a failure of 240% (Figure S8, Supporting Information). Across different stretchable substrates with varying modulus, the BOIEFI structure demonstrated a remarkable enhancement in stretchability compared to the RCI system.

2.3. Mechanical Behavior of the BOIEFI

The optimized BOIEFI achieves high stretchability through its primary and secondary root configuration. Primary roots efficiently distribute stress, thereby delaying interfacial failure, while secondary roots function as flexible mechanical interlocks to prevent such failure. In the BOIEFI structure, each secondary root moves in the direction of strain, exhibiting flexible deformation. As strain increases, the secondary roots positioned at the upper area sequentially undergo maximum allowable bending. Once the uppermost area's secondary roots reach a certain bending deformation point, the bending process begins in the secondary roots located in the below area (**Figure 3a,b**). This sequential process continues until the entire secondary root structure reaches its bending limits, ultimately leading to interfacial failure.

The strain distribution within the BOIEFI was measured and analyzed during the tensile test to evaluate the impact of the root design on stretchability. Due to insufficient adhesion between PI and Ecoflex, interfacial failure occurred at a strain of 40% in the RCI (Figure 3c). Crack propagation along the interface was observed at strains below 80% due to stress concentration at the region of interfacial failure. The integration of the optimized BOIEFI effectively enhances the stretchability of the hybrid electronics platform. Through Digital Image Correlation (DIC) experiments, the effective gripping effect of BOIEFI roots could be demonstrated. As strain increased, BOIEFI showed no cracking along the boundary between the secondary root and Ecoflex, sustaining strain levels up to 400% (Figure 3d). Due to the large strain values applied during testing, the peak local strain was demonstrated as a representative measure to capture the mechanical response in regions with the highest deformation. Finally, crack propagation in the BOIEFI structure was observed at an applied strain of 550% although their strain distribution could not be measured because the DIC experiment had limitations in capturing high strain during crack propagation (Figure S9, Supporting Information).

To further elucidate the mechanism of achieving high stretchability, finite element analysis (FEA) was performed on omnidirectional models of an RCI, a primary root, and a secondary root. For a 18-fold rotationally symmetric structure, displacement-controlled tensile loading was applied in the *y*-direction to

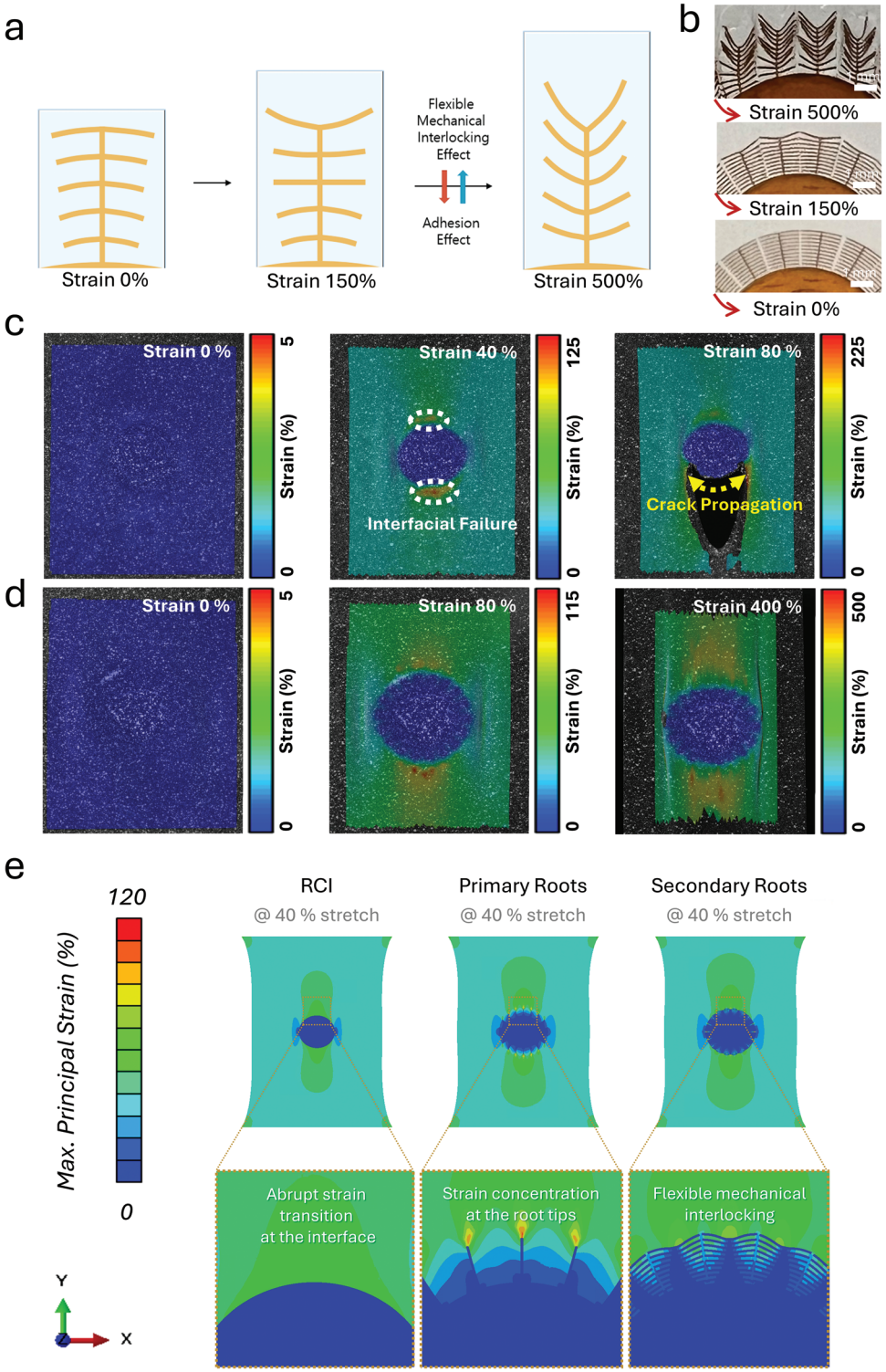

Figure 3. Investigation of the mechanical behavior of the BOIEFI. a) Schematic illustration of BOIEFI working mechanism with flexible mechanical interlocking and adhesive effects. b) Photographs of BOIEFI within stretchable substrate under strain values of 0%, 150%, and 500%, respectively. c,d) Digital image correlation (DIC) image showing interfacial failure and crack propagation in c) RCI, d) BOIEFI. e and f) Finite element analysis (FEA) for investigating e) small-scale interfacial crack opening and f) bending behavior of secondary roots (deformation scale factor: 3).

investigate the detailed strain distribution and the deformation behavior of root structures. Detailed information regarding the FEA model is provided in Figure S10 (Supporting Information) and the Experimental Section. Figure 3e presents the maximum principal strain plot at the overall stretch of 40%. From the strain plot, it is observed that the root structure effectively reduces the strain of Ecoflex at the interface. While abrupt strain transitions occur at the interface of the circular RCI structure, the root structure facilitates the formation of graded strain distributions. This gradual strain variation helps to mitigate stress concentrations, enhancing mechanical stability and interfacial robustness under deformation through the root structure. Moreover, while primary root structures may be vulnerable to delamination due to strain concentration at the root tips, secondary root structures mitigate the issue with sequential bending of secondary roots in the direction of loading (Figure S11, Supporting Information). To evaluate the adhesion characteristics between Ecoflex and PI under repetitive mechanical loading, a cyclic peeling test was conducted (Figure S12, Supporting Information). During the first cycle, the adhesion test exhibited a high adhesion force; however, in subsequent cycles, a reduction in adhesion force was observed (Figure S13, Supporting Information), indicating progressive degradation of interfacial adhesion under repeated loading conditions. Despite this reduction, the flexible mechanical interlocking behavior of the secondary root structures was found to be highly effective in maintaining structural integrity and mechanical performance, even under conditions of reduced adhesion at the interface caused by cyclic mechanical loading (Figure S14, Supporting Information). From simulating the same FEA models but with uniformly distributed microcracks at the interface and reduced adhesion, it is found that delamination occurs at the interface of RCI structure under strain of 33%, and delamination initiates and propagates from the root tips of primary roots structure under strain of 40%, while delamination was effectively suppressed for secondary root structures under the equivalent level of stretch. Thus, it is concluded from the FEA with two different interfacial properties that graded strain distribution along the primary root and sequential bending of secondary roots subsequently suppresses the opening and propagation of interfacial microcracks. The flexible mechanical interlocking effect from this bending behavior of secondary roots is deduced to further enhance stretchability by complicating the crack propagation path and dissipating the strain energy.

2.4. Mechanical Reliability of the BOIEFI

In addition to its remarkable stretchability, the optimized BOIEFI demonstrates excellent fatigue resistance over prolonged durations. Fatigue tests were performed on RCI at 50% strain and on BOIEFI at 150% strain. Interfacial failure was identified by a decrease in applied stress under the same strain levels.[36] During the initial phase of the fatigue experiment, interfacial failure initiation was evident after the first cycle for RCI (**Figure 4a**). Subsequently, accelerated interfacial failure was observed in the RCI after 90 cycles, as indicated by a noticeable drop in the graph. In contrast, BOIEFI exhibited remarkably strong interfacial durability even after maintaining its structural integrity even after 1000 cycles at higher strain levels (Figure 4b).

To verify the mechanical robustness of the omnidirectional BOIEFI under twisting conditions, we subjected both RCI and BOIEFI to the cyclic tensile strain of 60% at twisting angles of 180° and 360° (Figure 4c). Figure 4d illustrates the relative change in modulus over cycles. When cyclically stretched at a twisting angle of 180° for RCI, the E/E_0 ratio dropped below 0.85, indicating interfacial failure occurred around the 5^{th} cycle. Subsequently, the E/E_0 ratio continued to decrease until the complete failure of the RCI occurred after ≈20 cycles. In contrast, the E/E_0 ratio of the BOIEFI exhibited a slight decrease over 1000 cycles at twisting angles of 180° and 360° which demonstrates an initial stabilization period followed by a stable period. To evaluate failure under poking deformation at 50% strain, cyclic pressure with a depth of 16 mm (initial pressure: 1.50 kPa, compressive force: 0.38 N) was applied to the RCI and BOIEFI embedded in Ecoflex (Figure 4e). Figure 4f depicts the variation in pressure (P/P_0) over the number of applied poking cycles. For RCI, interfacial failure occurs at the 20th poking cycle, as shown in the inset image in Figure 4f. In contrast, the BOIEFI maintained a reliable interface throughout the 1000 cycles. In summary, fatigue tests involving stretching, twisting, and poking indicate that the BOIEFI effectively inhibits crack propagation at the interface under repeated application of diverse physical deformation. These findings highlight the potential of BOIEFI to enhance hybrid electronics capabilities and significantly broaden its applicability across a wide range of practical scenarios such as human-machine interface, health monitoring, and displays, particularly those involving extreme mechanical loading conditions.

2.5. Hybrid Electronics Platforms with BOIEFI

Applications of hybrid electronics platforms, including stretchable LED arrays and human-machine interface devices are demonstrated with BOIEFI. To construct hybrid electronic devices, intrinsically stretchable electrodes based on Ag flakes and Ecoflex, which exhibit excellent performance under excessive stretching, were used. The electrodes were printed onto the platform using screen printing with a polyethylene terephthalate (PET) mask (**Figure 5a**). To investigate the electrical response of the fabricated platform, an electrical stability experiment was conducted for configurations without an island, with RCI, and with the optimized BOIEFI, as shown in Figure 5b. The intrinsically stretchable electrode without an island exhibits electrical failure at 800% strain due to elastomer failure. While the RCI experienced electrical failure at ≈90% strain, the optimized BOIEFI design shows electrical failure at ≈540% strain. Although the bare elastomer demonstrated the highest strain at failure, this structure is impractical for real-world applications because it cannot integrate rigid or flexible electronic components. In contrast, the elastomer with the optimized BOIEFI is well-suited for demonstrating hybrid electronics because it not only provides sufficient stretchability and electrical conductivity but also features islands capable of integrating various electronic components.

Then, an array of the optimized BOIEFI was used to fabricate a stretchable LED array. The 4 × 4 island arrays were prepared to integrate a stretchable LED array (Figure 5c and

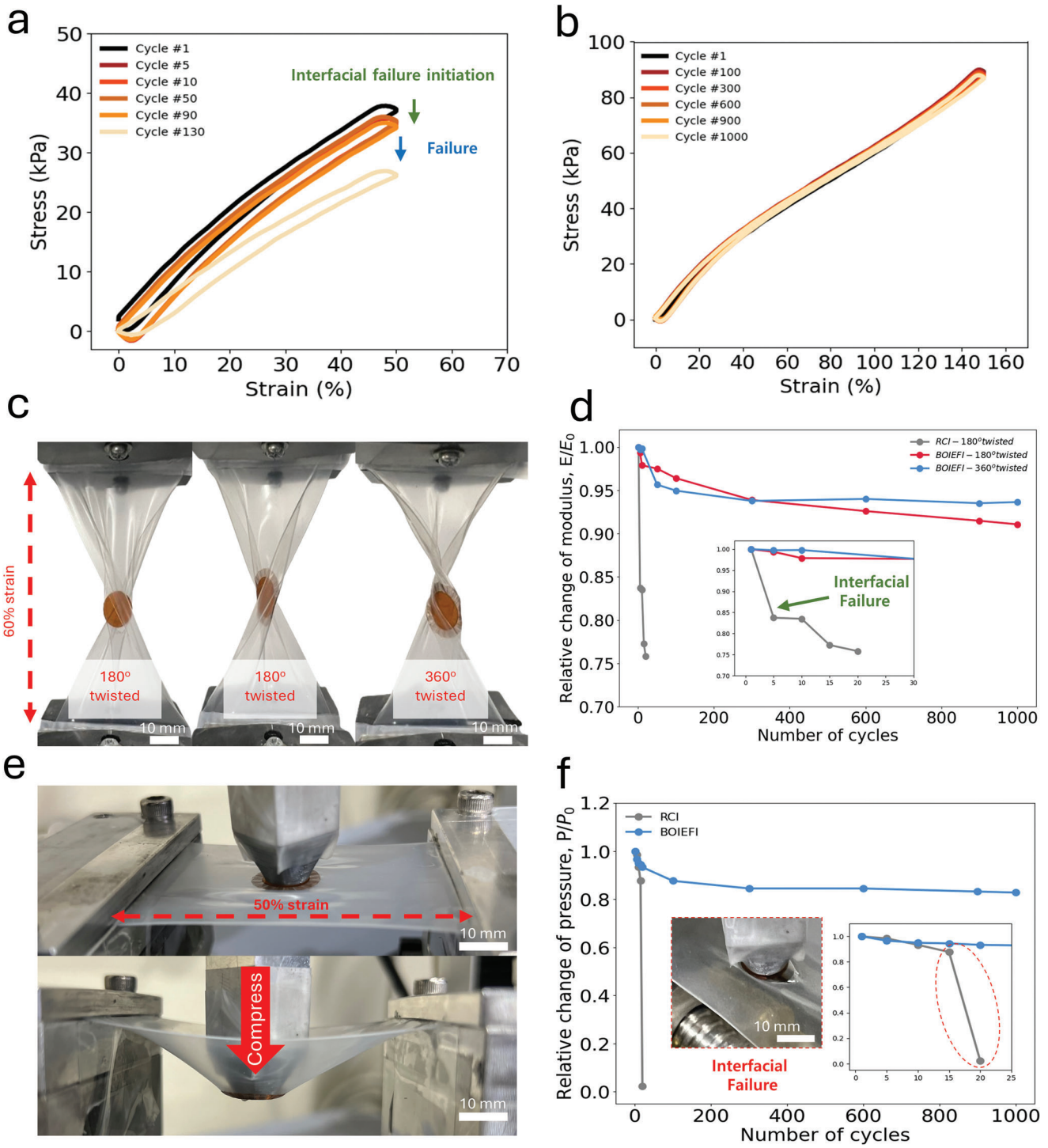

Figure 4. BOIEFI under diverse physical deformation modes. a,b) Stress versus strain graph of a) RCI b) BOIEFI under cyclic strain of 50% and 150%. c) Photographs of twisted RCI (180o) and BOIEFI (180o and 360o) for cyclic strain of 60%. d) Relative change of modulus (E/E0) versus cycles for twisted strain experiment of RCI and BOIEFI. The inset demonstrates a zoom-in of the curve at 0 to 30 cycles. e) Photographs of BOIEFI with 60% strain under cyclic pressure (initial force: 0.38 N, repeated compression depth: 16 mm). f) Relative change of pressure (*P*/*P*0) versus cycle for RCI and BOIEFI under cyclic poking. The inset on the right provides a zoom-in of the curve at 0 to 25 cycles. The inset on the left demonstrates the failure of RCI after 15 cycles.

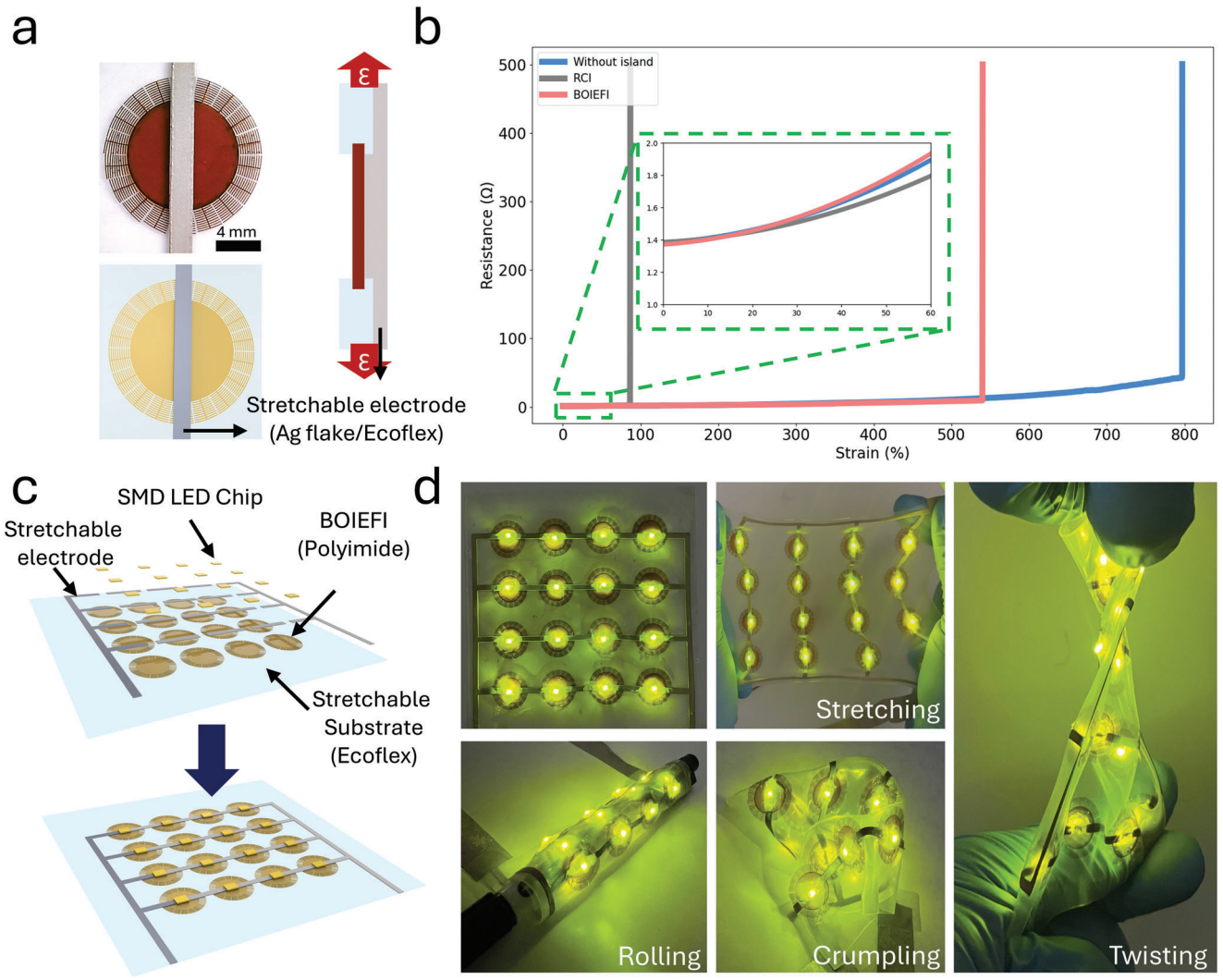

Figure 5. Stretchable Hybrid Electronics application of BOIEFI. a) Photograph (upper image) and schematic illustration (lower image) of the intrinsically stretchable electrode on the BOIEFI platform. b) Resistance versus strain for the printed intrinsically stretchable electrode on different design cases: without island, RCI, and BOIEFI. The inset demonstrates a zoom-in of the curve at 0% to 40% strain. c) Schematic illustration of stretchable LED array. d) Photograph of the fabricated stretchable LED array under physical deformations (stretching (100% strain), rolling, crumpling, and twisting).

Experimental Section). The islands were embedded into the Ecoflex, and stretchable electrodes were subsequently printed using the screen-printing method with a prepared mask (Figure S15, Supporting Information). The prepared sample was detached from the glass substrate, and SMD LED chips were mounted onto each island. The components were then secured firmly with a silicone-based adhesive. The fabricated stretchable LED array shows robust performance under multiple physical deformation modes, such as stretching (≈100% strain), rolling (radius of 5 mm), crumpling, and twisting (180°) (Figure 5d; Movies S1, S2, Supporting Information).

For effective and practical applications of stretchable hybrid electronics platforms such as in virtual reality/augmented reality, human-machine interfaces, and health monitoring, it is crucial to realize the multi-functionality of the integrated system beyond just ensuring the reliable operation of individual components. In **Figure** 6a, a multifunctional and stretchable human-machine interface device (s-HMI Device) was demonstrated. The s-HMI device includes four CNT-based soft pressure sensors and four rigid LEDs that are mounted onto the BOIEFI. The fabricated s-HMI device exhibited stable performance under various physical deformation modes such as stretching and twisting applied to the entire device as shown in Figure 6b and Movie S3 (Supporting Information). As a wearable device application, the s-HMI device could function under 300% strain, providing visual directional information through LEDs and controlling the directions by CNT-based soft pressure sensors. Figure S16 (Supporting Information) and the Experimental Section illustrate and describe the system for establishing the s-HMI device. It was utilized to control the traditional snake game while simultaneously achieving visual directional information from the device (Figure 6c and Movie S4, Supporting Information). Simulating the functionality of keyboard arrow keys, pressing the CNT-based soft pressure sensor directed the snake to move down, left, up, or right.

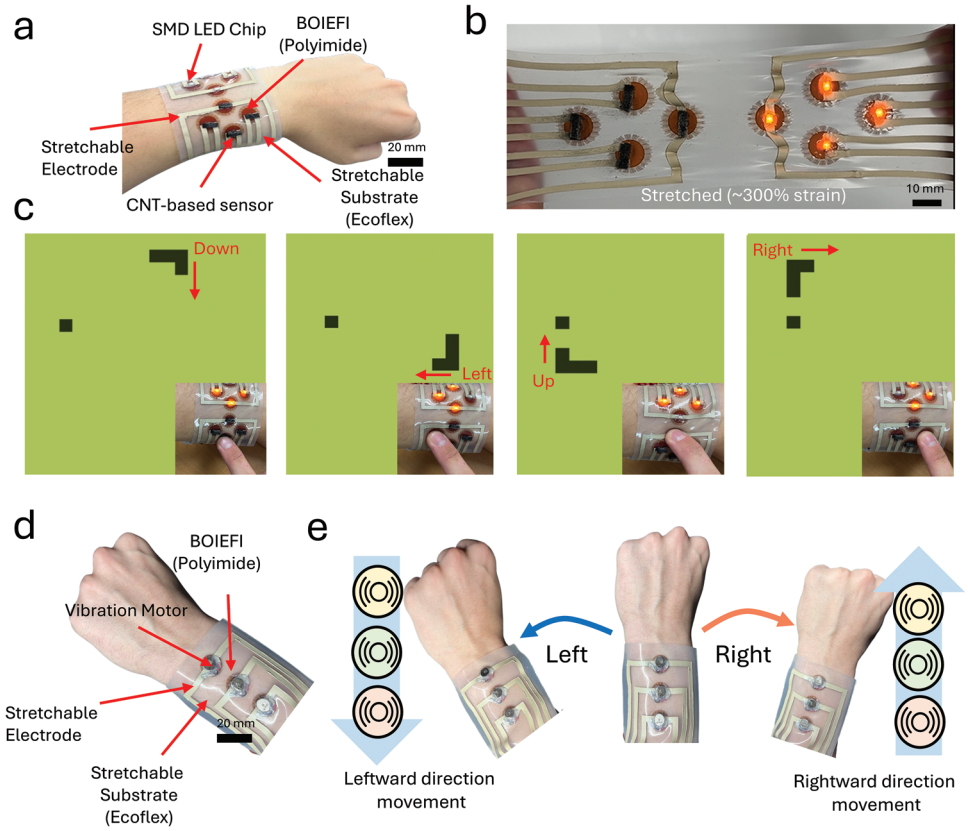

Figure 6. Stretchable Human-Machine Interface and Haptic Device with BOIEFI. a) Photograph of the fabricated Stretchable Human-Machine Interface Device (s-HMI Device) b) Photograph of the s-HMI Device under 300% strain. c) Photographs of the computer screen of controlling traditional snake game by s-HMI Device. The insets show the photographs of the s-HMI Device corresponding to each direction. d) Photograph of the fabricated Stretchable Haptic Device e) Photographs and illustration of haptic feedback and directional movement.

The corresponding LEDs light up to visually indicate each direction. Moreover, the s-HMI Device demonstrates stable operation under stretching (300% strain) as shown in Movies S5, S6 (Supporting Information). Ultimately, we successfully developed an s-HMI Device with BOIEFI integrating soft pressure sensors and rigid LEDs, achieving broad applicability across diverse areas.

A stretchable haptic device was developed by integrating vibration motors onto the BOIEFI platform (Figure 6d). These integrated vibration motors are programmed to convey directional information through controlled vibration patterns. The directional control of the vibration motors is managed using an Arduino microcontroller. Specifically, three vibration motors are configured to deliver directional movement instructions based on sequential vibration patterns. For instance, a vibration sequence that starts from the top motor and progresses downward indicates a leftward directional movement. Conversely, a sequence that begins from the bottom motor and moves upward signifies a rightward directional movement (Figure 6e; Movie S7, Supporting Information). This programmable vibrational feedback system enables the stretchable haptic device to be employed in a variety of applications requiring directional guidance. Furthermore, as demonstrated in Movie S8 (Supporting Information), the haptic device operates effectively under 200% strain, showcasing its ability to function in highly stretchable conditions. This remarkable stretchability expands the potential applications of BOIEFI, enabling diverse and multifunctional uses in flexible and wearable technologies.

3. Conclusion

Hybrid electronics represent a key technology that should be advanced for the practical deployment of stretchable electronics. Additionally, to ensure the practical implementation of hybrid electronics across various real-world applications, these devices need to demonstrate exceptional durability in demanding environments. In this study, we developed BOIEFIs for the establishment of hybrid electronics that can achieve highly stretchable and durable performance under various physical deformation. Our approach involved engineering a flexible-to-stretchable interface inspired by biological principles, incorporating both primary and secondary roots of plants. These roots facilitate stress distribution and flexible mechanical interlocking, enabling high stretchability and endurance through various deformations, including stretching, rolling, crumpling, and twisting. While these achievements were demonstrated with a relatively simple design in this study, there remain significant opportunities remain for advancing the proposed hybrid electronics platform. For example, in nature, plant roots exhibit complex 3D structures that provide strong gripping effects. Mimicking these 3D complex structures

in future work could enhance the stability of the interface and improve the gripping effect on the stretchable substrate. Despite the simplicity of the current design, we have demonstrated the practicality of the developed stretchable hybrid electronics platform by successfully integrating LEDs (rigid components) onto the BOIEFI (flexible substrate). Additionally, we developed a stretchable human-machine interface (s-HMI) device that functions as a keyboard directional input and provides visual feedback by integrating soft pressure sensors and LEDs into the platform. The BOIEFI represents a novel approach for advancing hybrid electronics, with potential applications in displays, extended reality, electronic skin, healthcare devices, and more.

4. Experimental Section

Fabrication Process for Tensile Test: The root designs were created with 3D computer-aided design (CAD) software (Fusion 360, Autodesk, USA). The BOIEFI specimens were fabricated using UV laser-cutting. Once modeled, the 3D CAD file was converted to a DXF format and imported into the UV laser-cutting software (KEYENCE Marking Builder, Japan). Polyimide (PI) film (SKC KOLON PI, Korea) was prepared and placed into the UV laser-cutting machine (MD-U1000C, KEYENCE, Japan). The UV laser cutting parameters included a laser power of 80% (2.4 W), a scan speed of 300 mm s^{-1}, a pulse frequency of 40 kHz, and a total of 20 passes. After laser cutting, the patterned PI was detached from the PI film.

A releasing agent (ER-200, Smooth-On Inc., USA) was applied to the soda-lime glass (Nippon Sheet Glass, Japan) to facilitate the release of the Ecoflex-0030. The Ecoflex-0030 was prepared by mixing its components, A and B, in a planetary mixer (Thinky ARM-310, USA) with a ratio of 1:1 for a mixing time of 2 min at 2000 rpm and a defoaming time of 10 s at 2200 rpm. After each mixing of the elastomer, the mixture was degassed in a vacuum chamber for 10 mins. The soda-lime glass was spin-coated with the prepared Ecoflex-0030 via spin-coating (900 rpm, 20s) and subsequently cured at 80 °C for 30 min. Subsequently, the prepared patterned PI was placed onto the Ecoflex-0030. Subsequently, an additional quantity of Ecoflex-0030 was prepared and spin-coated (500 rpm, 20s) in order to encapsulate the patterned PI. The specimen was then subjected to a curing process at 80 °C for a period of 30 min. Subsequently, the specimen was prepared by cutting it into a size of 42 × 42 mm. Finally, the specimen was prepared for the tensile test, which was conducted in order to identify any interfacial failure between the flexible and stretchable substrates.

Tensile-Related Tests: In all tensile tests, a universal testing machine (AG-X plus, Shimadzu, Japan) and a load cell (SBL-1KN, Shimadzu, Japan) capable of measuring up to 1 kN force were employed to quantify the applied force. Pneumatic flat grips (Shimadzu, Japan) were employed to ensure secure grasping of the specimens for each experiment. The speed was set to 50 mm min^{-1} for each test. In order to ascertain the strain at failure of the omnidirectional design (Figure S1, Supporting Information), the specimen was subjected to a vertical directional strain. In each test, the specimen's position was rotated by 60°.

While the complete embedment of BOIEFI specimens in Ecoflex enabled visual detection of interfacial failures between flexible and stretchable substrates, it also created challenges for quantitative measurement with the load drop method. The load drop method referred to a sudden decrease in the applied load, typically indicating the onset of crack initiation, leading to material failure. To overcome this, Ecoflex was removed from the BOIEFI specimen using a 9 mm circular punch, allowing for tensile tests to be conducted (Figure S17, Supporting Information). This approach allowed interfacial failure to be quantitatively demonstrated using the load-drop method.[30,37]

Digital Image Correlation for Strain Mapping: The strain distribution on the surface of the BOIEFI specimens was calculated and analyzed using a commercial digital image correlation (DIC) algorithm program (ARAMIS, Gesellschaft für Optische Messtechnik mbH) with an error of 0.005% for strain measurement. For the purpose of strain measurement, white speckle patterns were randomly generated on the surface of the BOIEFI specimens using a commercial ceramic spray (SF 7900, LOCTITE, Germany). Two charge-coupled device (CCD) cameras (6 million pixels) were calibrated to measure the appropriate area (30 × 24 mm). The tensile test was conducted at a speed of 50 mm min^{-1} using a universal testing machine (AGS-X, SHIMADZU, Japan), and the two CCD cameras captured images at 3 Hz. The equivalent Mises strain distribution within the boundary region between the PI root and Ecoflex-0030 was analyzed by applying the interpolation method, which calculated the strain in the boundary region as the average value of the strains of the PI root and Ecoflex-0030.

Finite Element Analysis for Investigating Small-Scale Behavior: The comparative investigation for the small-scale mechanical behavior of the BOIEFI was performed using commercial finite element analysis software (Abaqus v 6.26, Dassault Systems, France). While the PI root structures were assumed to be purely elastic (E: 2.5 GPa, v: 0.34), the Ecoflex soils were modeled to be hyperelastic by adopting coefficients of the Ogden model (μ1: 0.01690, α1: 1.3, μ2: 0.00008, α2: 5.0, μ3: 0.00100, α3: -2.0, D1: 1.1560, D2: 0.0001, D3: 0.0000). Each 2D deformable solid model for the root-mimicking PI and soil-mimicking Ecoflex structures consisted of ≈4000 and ≈30000 CPS4R (4-node bilinear plane stress quadrilateral, reduced integration, hourglass control) elements, respectively. The interfaces were set to be perfectly bonded for models investigating detailed strain distribution of RCI and root structures, while the possible growth of interfacial microcracks (length: ≈ 20 μm) was modeled by adopting the virtual crack closure technique (VCCT) with a critical energy release rate of 0.1 J m^{-2} for models investigating delamination of RCI and root structures under reduced adhesion.

Fabrication of Intrinsically Stretchable Electrode: The electrode used in this study was based on an Ag flake/Ecoflex combination, as previously described in a related study.[36] MIBK (4-methyl-2-pentanone) (Daejung Chemical & Metals, Korea) and Ecoflex-0030 were combined in a 3:3 ratio using a planetary mixer (mixing time of 2 min and a defoaming time of 10 s). Ag flakes (Daejoo Electronic Materials, Korea) were then added to the obtained mixed solution in a ratio of 14, after which the solution was mixed again with the planetary mixer at the same conditions previously described. Subsequently, the final solution of Ag flakes, Ecoflex, and MIBK was screen-printed on the prepared islands through a polyethylene terephthalate (PET) mask with a thickness of 200 μm. The MIBK solvent was subjected to evaporation at 80 °C for 1 h. Thermal sintering of the Ag flake/Ecoflex solution was conducted at 110 °C for a period of 2 h, resulting in an electrical conductivity of 4006 S cm^{-1}.

Electrical Stability Test of Intrinsically Stretchable Electrode: To assess the electrical stability of intrinsically stretchable electrodes integrated into the stretchable hybrid electronics platform, a woven conductive fabric (Shzhou Wanhe Electronic, China) was employed to connect the intrinsically stretchable electrodes to the Arduino Due. The resistance of the intrinsically stretchable electrode was quantified by utilizing a reference resistor in series to create a voltage-dividing circuit.

Fabrication of Stretchable LED Array: Ecoflex-0030 was spin-coated onto a 150 × 150 mm soda-lime glass substrate. The BOIEFI was placed in a 4 × 4 formation with equal spacing on the Ecoflex-0030. A second layer of Ecoflex-0030 was spin-coated onto the islands for embedment. The Ag flake/Ecoflex/MIBK solution was screen-printed on the islands using a PET mask. After curing the intrinsically stretchable electrode, the sample was detached from the glass. SMD LED chips (HSUKWANG, China) were mounted on each island and secured with Silpoxy (Smooth-On Inc., USA). Woven conductive fabric (Shzhou Wanhe Electronic, China) was used to connect the intrinsically stretchable electrode to electric wires. A 12 V bias was applied to activate the SMD LED chips.

Fabrication of CNT-Based Soft Pressure Sensor: The CNT-based soft pressure sensor used in this study was described previously in a related study.[38] To fabricate a porous PDMS sponge, a sugar template (15 mm × 15 mm × 15 mm) was immersed in degassed polydimethylsiloxane prepolymer (PDMS, Sylgard 184, Dow Corning Co., with a 10:1 matrix-to-curing agent mass ratio). The liquid PDMS prepolymer was infiltrated into the sugar template within a vacuum chamber for 1 h and then cured in a convection oven at 70 °C for 2 h. The composite of sugar and cured PDMS was then cut into a thin slice, ≈3 mm thick, using sandpaper. This

slice was immersed in deionized water at 60 °C for 1 h to dissolve the sugar, resulting in a porous PDMS sponge (15 mm × 15 mm × 3 mm).

Subsequently, the obtained PDMS sponge was treated with oxygen plasma for 10 min. A mixture of 0.25 g of multiwalled carbon nanotubes (MWCNTs) (Hyosung, with a diameter of 16 ± 3.6 nm and length of 5–20 μm) was dispersed in 100 mL of isopropyl alcohol (IPA). After vortex mixing for 1 h and ultrasonication for an additional hour, a homogeneous 0.25 wt. % CNT-IPA dispersion was prepared. The plasma-treated PDMS sponge was then immersed in the CNT-IPA dispersion and repeatedly squeezed to coat the surfaces of the PDMS backbone with CNTs. After the complete evaporation of the IPA solvent, the prepared sample was rinsed in deionized water and dried in a convection oven at 50 °C for 1 h.

Fabrication of Stretchable Human-Machine Interface Device: These experiments were approved by the institutional review board (IRB) of the Korea Advanced Institute of Science and Technology (KAIST) (IRB no. KH2024-200). Before processing the fabrication, a PET mask was designed and fabricated with UV laser-cutting software. Ecoflex-0030 was spin-coated onto a 100 × 100 mm soda-lime glass substrate. The fabricated PET mask was attached to the spin-coated soda-lime glass substrate to align the position of the BOIEFI. After placement of the BOIEFI, a second layer of Ecoflex-0030 was spin-coated for embedment. The Ag flake/Ecoflex/MIBK solution was applied with screen-printing onto the BOIEFI using the fabricated PET mask. After curing the intrinsically stretchable electrode, the sample was detached from the glass. The fabricated CNT-based soft pressure sensor and LEDs were mounted onto the intrinsically stretchable electrodes using Ag epoxy (MG Chemicals Ltd., 8331S, Canada) as a conductive adhesive. The Ag epoxy was sintered after mounting using a convection oven at 60 °C for 20 min. Silpoxy was applied to securely attach the LEDs to the device. The fabricated s-HMI Device was connected to the Arduino by using alligator clips. The detailed connection schematic to the Arduino of the fabricated s-HMI Device can be found in Figure S16 (Supporting Information).

Supporting Information

Supporting Information is available from the Wiley Online Library or from the author.

Acknowledgements

I.P. was supported by the National Research Foundation of Korea (NRF) grant funded by the Korean government (MSIT) (No. 2021R1A2C3008742). H.J.K. was supported by the Institute of Information & communications Technology Planning & Evaluation (IITP) grant funded by the Korean government (MSIT) (No. 2022-0-00025) and Korea Evaluation Institute of Industrial Technology (KEIT) grant funded by the Korea government (MOTIE) (No. RS-2022-00154781).

Conflict of Interest

The authors declare no conflict of interest.

Author Contributions

O.G. and I.P. led the development of the concepts, designed the experiments, and interpreted the results; M.S. carried out the simulation of design; C.Y.G. conducted the experiment on DIC analysis; O.G. led the experimental work with support from Jihyeon A., K.L.; Junseong A. H.J.K, I.P. directed the project.

Data Availability Statement

The data that support the findings of this study are available in the supplementary material of this article.

Keywords

bioinspired structure, flexible-to-stretchable interface, interfacial engineering, stretchable human-machine interface device, stretchable hybrid electronics

Received: October 31, 2024
Revised: January 5, 2025
Published online:

[1] S. Choi, H. Lee, R. Ghaffari, T. Hyeon, D. H. Kim, *Adv. Mater.* **2016**, *28*, 4203.
[2] M. S. Kim, Y. Lee, J. Ahn, S. Kim, K. Kang, H. Lim, B. S. Bae, I. Park, *Adv. Funct. Mater.* **2023**, *33*, 2208792.
[3] S. Y. Hong, Y. H. Lee, H. Park, S. W. Jin, Y. R. Jeong, J. Yun, I. You, G. Zi, J. S. Ha, *Adv. Mater.* **2016**, *28*, 930.
[4] Y. Cao, G. Zhang, Y. Zhang, M. Yue, Y. Chen, S. Cai, T. Xie, X. Feng, *Adv. Funct. Mater.* **2018**, *28*, 1804604.
[5] J. Choi, C. Han, S. Cho, K. Kim, J. Ahn, D. Del Orbe, I. Cho, Z.-J. Zhao, Y. S. Oh, H. Hong, *Sci. Adv.* **2021**, *7*, eabj0694.
[6] O. Gul, K. Kim, J. Gu, J. Choi, D. Del Orbe Henriquez, J. Ahn, I. Park, *ACS Appl. Electron. Mater.* **2021**, *3*, 4027.
[7] O. Gul, J. Kim, K. Kim, H. J. Kim, I. Park, *Adv. Mater. Technol.* **2024**, *9*, 2302134.
[8] D. W. Kim, M. Kong, U. Jeong, *Adv. Sci.* **2021**, *8*, 2004170.
[9] J. A. Rogers, T. Someya, Y. Huang, *Science.* **2010**, *327*, 1603.
[10] Z. Xue, H. Song, J. A. Rogers, Y. Zhang, Y. Huang, *Adv. Mater.* **2020**, *32*, 1902254.
[11] S. Hou, C. Chen, L. Bai, J. Yu, Y. Cheng, W. Huang, *Small.* **2024**, *20*, 2306749.
[12] X. Liu, Q. Wang, S. Zhou, S. Feng, Y. Wei, F. Bu, K. Wang, J. Wang, B. Zhang, C. Guan, *Adv. Mater.* **2024**, *36*, 2407886.
[13] C. A. Silva, J. Lv, L. Yin, I. Jeerapan, G. Innocenzi, F. Soto, Y. G. Ha, J. Wang, *Adv. Funct. Mater.* **2020**, *30*, 2002041.
[14] S. Y. Hong, M. S. Kim, H. Park, S. W. Jin, Y. R. Jeong, J. W. Kim, Y. H. Lee, L. Sun, G. Zi, J. S. Ha, *Adv. Funct. Mater.* **2019**, *29*, 1807679.
[15] D. Qi, K. Zhang, G. Tian, B. Jiang, Y. Huang, *Adv. Mater.* **2021**, *33*, 2003155.
[16] S. Xu, Y. Zhang, J. Cho, J. Lee, X. Huang, L. Jia, J. A. Fan, Y. Su, J. Su, H. Zhang, *Nat. Commun.* **2013**, *4*, 1543.
[17] A. T. Haque, D. Hwang, M. D. Bartlett, *Adv. Mater. Technol.* **2022**, *7*, 2101241.
[18] S. Kim, Y. S. Oh, K. Lee, S. Kim, W. Y. Maeng, K. S. Kim, G. B. Kim, S. Cho, H. Han, H. Park, *Small.* **2023**, *19*, 2206839.
[19] S. Cho, H. Han, H. Park, S.-U. Lee, J.-H. Kim, S. W. Jeon, M. Wang, R. Avila, Z. Xi, K. Ko, *npj Flex. Electron.* **2023**, *7*, 8.
[20] Y. Morikawa, S. Yamagiwa, H. Sawahata, R. Numano, K. Koida, M. Ishida, T. Kawano, *Adv. Healthcare Mater.* **2018**, *7*, 1701100.
[21] B. Jang, S. Won, J. Kim, J. Kim, M. Oh, H. J. Lee, J. H. Kim, *Adv. Funct. Mater.* **2022**, *32*, 2113299.
[22] Y. S. Oh, J.-H. Kim, Z. Xie, S. Cho, H. Han, S. W. Jeon, M. Park, M. Namkoong, R. Avila, Z. Song, *Nat. Commun.* **2021**, *12*, 5008.
[23] Z. Rao, Y. Lu, Z. Li, K. Sim, Z. Ma, J. Xiao, C. Yu, *Nat. Electron.* **2021**, *4*, 513.
[24] M. S. Kim, S. Kim, J. Choi, S. Kim, C. Han, Y. Lee, Y. Jung, J. Park, S. Oh, B.-S. Bae, *ACS Appl. Mater. Interfaces.* **2021**, *14*, 1826.
[25] R. Libanori, R. M. Erb, A. Reiser, H. Le Ferrand, M. J. Süess, R. Spolenak, A. R. Studart, *Nat. Commun.* **2012**, *3*, 1265.
[26] E. Oh, J. Byun, B. Lee, S. Kim, D. Kim, J. Yoon, Y. Hong, *Adv. Electron. Mater.* **2017**, *3*, 1.
[27] N. Matsuhisa, M. Kaltenbrunner, T. Yokota, H. Jinno, K. Kuribara, T. Sekitani, T. Someya, *Nat. Commun.* **2015**, *6*, 7461.

[28] N. Naserifar, P. R. LeDuc, G. K. Fedder, *Adv. Mater.* **2016**, *28*, 3584.
[29] M. Kim, S. Hong, J. J. Park, Y. Jung, S. H. Choi, C. Cho, I. Ha, P. Won, C. Majidi, S. H. Ko, *Adv. Mater.* **2024**, *36*, 2313344.
[30] J. C. Yang, S. Lee, B. S. Ma, J. Kim, M. Song, S. Y. Kim, D. W. Kim, T.-S. Kim, S. Park, *Sci. Adv.* **2022**, *8*, eabn3863.
[31] C. Zhu, R. Li, X. Chen, E. Chalmers, X. Liu, Y. Wang, B. B. Xu, X. Liu, *Adv. Sci.* **2020**, *7*, 2002009.
[32] J. Xue, Y. Zou, Y. Deng, Z. Li, *EcoMat.* **2022**, *4*, e12209.
[33] D. Liu, C. Huyan, Z. Wang, Z. Guo, X. Zhang, H. Torun, D. Mulvihill, B. B. Xu, F. Chen, *Mater. Horiz.* **2023**, *10*, 2800.
[34] D. Liu, H. Zhou, Y. Zhao, C. Huyan, Z. Wang, H. Torun, Z. Guo, S. Dai, B. B. Xu, F. Chen, *Small.* **2022**, *18*, 2203258.
[35] T. J. Wallin, L.-E. Simonsen, W. Pan, K. Wang, E. Giannelis, R. F. Shepherd, Y. Mengüç, *Nat. Commun.* **2020**, *11*, 4000.
[36] S. H. Kim, S. Jung, I. S. Yoon, C. Lee, Y. Oh, J. M. Hong, *Adv. Mater.* **2018**, *30*, 1800109.
[37] Z. Liao, M. Hossain, X. Yao, R. Navaratne, G. Chagnon, *Polym. Test.* **2020**, *86*, 106478.
[38] S. Kim, M. Amjadi, T.-I. Lee, Y. Jeong, D. Kwon, M. S. Kim, K. Kim, T.-S. Kim, Y. S. Oh, I. Park, *ACS Appl. Mater. Interfaces.* **2019**, *11*, 23639.